Spin-incoherent Luttinger liquid of one-dimensional spin-1 Tonks-Girardeau Bose gases: Spin-dependent properties

H. H. Jen[1] and S.-K. Yip[1,2]

[1]*Institute of Physics, Academia Sinica, Taipei 11529, Taiwan*
[2]*Institute of Atomic and Molecular Sciences, Academia Sinica, Taipei 10617, Taiwan*

Spin-incoherent Luttinger liquid (SILL) is a different universal class from the Luttinger liquid. This difference results from the spin incoherence of the system when the thermal energy of the system is higher than the spin excitation energy. We consider one-dimensional spin-1 Bose gas in the SILL regime and investigate its spin-dependent many-body properties. In Tonks-Girardeau limit, we are able to write down the general wave functions in a harmonic trap. We numerically calculate the spin-dependent (spin-plus, minus, and zero) momentum distributions in the sector of zero magnetization which allows us to demonstrate the most significant spin-incoherent feature compared to the spinless or spin-polarized case. In contrast to the spinless Bose gas, the momentum distributions are broadened and in the large momentum limit follow the same asymptotic $1/p^4$ dependence but with reduced coefficients. While the density matrices and momentum distributions differ between different spin components for small N, at large N they approach each other. We show these by analytic arguments and numerical calculations up to $N = 16$.

I. INTRODUCTION

A plethora of studies on one-dimensional (1D) quantum systems of gaseous atoms [1] thrive recently due to the experimental achievements of 1D confined bosons [2–4]. Many studies focus on the ground-state properties of spinless bosons [5–7] such as spatial and momentum distributions [8–10], quantum magnetism in a spinful Bose gas [11–16], and low-energy excitations in the Luttinger liquid model [17,18]. Meanwhile, a spinful quantum system in the spin-incoherent regime [19] also provides a new avenue for studying 1D quantum many-body systems. This regime is termed as spin-incoherent Luttinger liquid (SILL) which forms a different universality class from the Luttinger liquid, where the temperature is high enough that different spin configurations can be regarded as degenerate while low enough that charge excitation is suppressed. For 1D spin-1 Bose gas with s-wave scattering lengths satisfying $|a_0 - a_2| \ll a_{0,2}$ [20], there exists a window of temperature for the gas in SILL regime. This happens since the sound velocity is much larger than the spin velocity.

In the crossover regime between Luttinger liquid and SILL, 1D fermions with tunable spins [21] and their high momentum tails [22] have been studied, which show an evident broadening in the momentum distributions [23,24]. Quantum criticality [25] and Pomeranchuk effect [26] in the spin-incoherent regime are also theoretically predicted in the two-dimensional Hubbard model. Here in contrast we investigate 1D spin-1 Bose gas in the SILL regime in a harmonic trap, which is studied only recently [27]. We shall focus on the Tonks-Girardeau (TG) regime [28,29] where the density is sufficiently low that the effective repulsion between particles can be regarded as infinite. TG spinor Bose gas is a special case of SILL since the exchange energy vanishes in this limit [13–16]. Therefore, TG gas automatically is in the regime of SILL. In TG gas limit, we can write down the exact spatial wave functions since bosons are fermionized and impenetrable due to effectively infinitely strong

atom-atom interactions. We then numerically calculate the momentum distributions for the three individual components of the spin-1 Bose gas (spin-plus, minus, and zero). These predictions can be measurable in spin-resolved matter-wave experiments, either the time-of-flight experiment [30–33] or Bragg scattering spectroscopy [34–39]. This system allows for better demonstrations of SILL physics which is within reach of present experimental conditions. As compared with electronic spin-1/2 systems [19,24], ultracold atom experiments not only provide controllable spatial dimensions but also tunable atom-atom interactions via Feshbach resonances, thus making our investigations testable in the quantum many-body systems.

In Ref. [27], we have derived the wave functions and density matrix for 1D spin-1 Bose gas in TG limit. We numerically calculate its momentum distributions, summed over spin components, up to six bosons. The momentum distributions are uniformly broadened as the number of bosons N grows. We have also derived the analytical large momentum (p) asymptotic in one-body momentum distributions, which shows the universal $1/p^4$ dependence. The coefficients of the asymptotic $1/p^4$ are also formulated for arbitrary N. Here we present the spin-dependent properties of density matrix in 1D spin-1 Bose gas in TG limit, and show the spin-dependent momentum distributions up to $N = 16$. We also obtain the spin-dependent coefficients of $1/p^4$ for asymptotic large p. Though the momentum distributions vary between different spin components for small N, they approach each other as N increases. We show this from the numerical results accompanied by analytical arguments in the large N limit.

The rest of the paper is organized as follows. In Sec. II we introduce the general wave functions for 1D spin-1 Bose gas. In Sec. III, we derive the general forms of density matrices for each spin component with individual spin function overlaps in SILL regime, and present the numerically calculated results using Monte Carlo integration method implemented with Gaussian unitary ensemble. In Sec. IV, we discuss the analytical derivation of high momentum asymptotic for each

053631-1

component, which we compare with numerically calculated momentum distributions. We also investigate the momentum distributions in large N limit using the method of steepest descent or stationery phase, and compare them with the numerical results. Finally, we conclude in Sec. V.

II. GENERAL WAVE FUNCTIONS IN TG LIMIT

Our effective Hamiltonian of ultracold 1D spin-1 Bose gas in TG limit can be expressed as [11,40,41]

$$H = \sum_{i=1}^{N} \left[-\frac{\hbar^2}{2m} \frac{\partial^2}{\partial x_i^2} + \frac{1}{2} m\omega^2 x_i^2 \right] \mathbb{I}_{\text{spin}}$$
$$+ \sum_{i<j} \delta(x_i - x_j) U_0 \mathbb{I}_{\text{spin}}, \quad (1)$$

where m and ω are respectively the mass of the bosons and the axial trap frequency. U_0 is the spin-independent interaction, which in TG limit becomes infinite. Here we have already ignored a spin-dependent interaction term since, in TG limit, all spin configurations are degenerate [13–16]. In general we can express the wave function of N bosons as

$$|\Psi\rangle = \sum_{s_1,s_2,\ldots,s_N} \psi_{s_1,s_2,\ldots,s_N}(\vec{x}) |s_1,s_2,\ldots,s_N\rangle, \quad (2)$$

where we denote $\vec{x} = (x_1,x_2,\ldots,x_N)$ and $|s_1,s_2,\ldots,s_N\rangle \equiv |\vec{s}\rangle$ as the spatial distributions and the spin configurations, respectively. Here we can label $s_i = +, -,$ or 0, respectively for spin-plus, minus, and zero components for the ith particle. The total wave function must satisfy the bosonic symmetry; therefore, it is sufficient to just consider the ordered region of $x_1 < x_2 < \cdots < x_N$, and we can obtain all other regions via permutations of this ordered region. In TG gas limit, the atoms become fermionized that their spatial wave functions take the Slater determinant form of noninteracting fermions. For the symmetrized spatial part of the wave function, we denote it as $\psi_{\vec{n}}^{\text{sym}}(\vec{x})$ which can be expressed in terms of the eigenfunctions $\phi_{n_j}(x_j)$ of the noninteracting fermions in a harmonic trap,

$$\psi_{\vec{n}}^{\text{sym}}(\vec{x}) = \frac{1}{\sqrt{N!}} \mathbb{A}[\phi_{n_1}(x_1), \phi_{n_2}(x_2), \ldots, \phi_{n_N}(x_N)]$$
$$\times \text{sgn}(x_2 - x_1) \text{sgn}(x_3 - x_2) \ldots$$
$$\times \text{sgn}(x_N - x_{N-1}). \quad (3)$$

We denote the sign function as sgn and the antisymmetrizer as $\mathbb{A}$ for later convenience. The orbital indices are

$(n_1, n_2, \ldots n_N)$, and the prefactor $\sqrt{N!}$ normalizes the wave function. For convenience we use the dimensionless forms of the eigenfunctions $\phi_n(y)$,

$$\phi_n(y) = \frac{1}{\sqrt{2^n n!}} \frac{1}{\pi^{1/4}} H_n(y) e^{-y^2/2}, \quad y \equiv x/x_{ho}, \quad (4)$$

where H_n are Hermite polynomials. The harmonic-oscillator length is $x_{ho} \equiv \sqrt{\hbar/(M\omega)}$, where ω is the trap frequency and M is the atomic mass.

To eventually evaluate the density matrix for say the "+" component, we need to obtain the wave-function amplitude where at least one particle has spin +. First we consider some degenerate and normalized spin configuration state $|\chi\rangle$ in some sector of magnetization, and the wave function can be expressed as $|\Psi\rangle = \psi_{\vec{n}}^{\text{sym}}(\vec{x})|\chi\rangle$. Take $N = 3$ for an example; we obtain the probability amplitude $\psi_{+,s_2,s_3}^{\text{sym}}(x,x_2,x_3)$ for the first particle having spin + when we project $|\Psi\rangle$ to $\langle s_1 = +, x_1 = x|$ in the ordered region of $x < x_2 < x_3$. To access the probability amplitudes in the other regions, we use the permutation operators P_{12} and P_{123} on the projected states, obtaining

$$x < x_2 < x_3, \quad \langle (+,s_2,s_3)|\chi\rangle,$$
$$x_2 < x < x_3, \quad \langle (s_2, +,s_3)|\chi\rangle = \langle P_{12}(+,s_2,s_3)|\chi\rangle,$$
$$x_2 < x_3 < x, \quad \langle (s_2,s_3,+)|\chi\rangle = \langle P_{123}(+,s_2,s_3)|\chi\rangle, \quad (5)$$

where we have suppressed the common $\psi_{\vec{n}}^{\text{sym}}(\vec{x})$ factors. Similar construction applies for other N's. In the next section we proceed to calculate the spin-dependent density matrices for spin-1 Bose gas in the SILL regime.

III. DENSITY MATRICES FOR SILL OF SPIN-1 BOSE GAS

The spin-dependent single-particle density matrix can be straightforwardly written down from the wave function described above. For example of the spin-plus component, we have

$$\rho_+(x,x') = N \sum_{\vec{s}'} \int d\bar{x} \, \psi_{+,\vec{s}'}^*(x,\bar{x}) \psi_{+,\vec{s}'}(x',\bar{x}), \quad (6)$$

where $\bar{x} \equiv (x_2,x_3,\ldots,x_N)$ and $\vec{s}' \equiv (s_2,s_3,\ldots,s_N)$. A factor of N represents N possible choices of x and x'.

Again we take $N = 3$ as an example, and consider only the region of $x < x'$ which is symmetric to $x > x'$. The spin-plus single-particle density matrix for $N = 3$ then becomes

$$\rho_+(x < x') = 3 \times 2 \left\{ \int_{x<x'<x_2<x_3} (E,E)_+ + \int_{x<x_2<x'<x_3} (E,P_{12})_+ + \int_{x<x_2<x_3<x'} (E,P_{123})_+ \right.$$
$$+ \int_{x_2<x<x'<x_3} (P_{12},P_{12})_+ + \int_{x_2<x<x_3<x'} (P_{12},P_{123})_+ + \left. \int_{x_2<x_3<x<x'} (P_{123},P_{123})_+ \right\}$$
$$\times \psi_{\vec{n}}^{\text{sym}*}(x,x_2,x_3) \psi_{\vec{n}}^{\text{sym}}(x',x_2,x_3) dx_2 dx_3, \quad (7)$$

where the parentheses () in various integral regions represent the spin function overlaps. Taking $(E,P_{12})_+$ as an example where E is the identical permutation operator, we define

$$(E,P_{12})_+ = \sum_{s_2,s_3} \langle E(+,s_2,s_3)|\chi\rangle \langle P_{12}(+,s_2,s_3)|\chi\rangle. \quad (8)$$

Similar forms apply to the other spin function overlaps in Eq. (7). Also the factor of 2 in Eq. (7) comes from the contribution of the integral region $x_2 > x_3$, where the spin function overlaps are the same as those with $x_2 < x_3$.

In the SILL regime, we average the above individual spin function overlaps by the total number of spin state configurations, which is denoted as $\mathrm{Tr}_\chi(E) \equiv \sum_\chi \langle \chi|E|\chi \rangle$. It is simply the trace (Tr) of the identical operator over all spin configurations $|\chi\rangle$ since $\langle\chi|E|\chi\rangle = 1$. We define the normalized spin function overlap in general as (using the same notation as the non-normalized one for simplicity)

$$(P_{12\ldots j}, P_{12\ldots k})_+ = \frac{\sum_{\vec{s}'}\langle P_{12\ldots j}(+,\vec{s}')|P_{12\ldots k}(+,\vec{s}')\rangle}{\mathrm{Tr}_\chi(E)}, \tag{9}$$

where $P_{12\ldots j}$ are j-particle permutation operators in the symmetric group S_N. To derive Eq. (9), we have used the identity $\sum_\chi |\chi\rangle\langle\chi| = 1$. $(P_{12\ldots j}, P_{12\ldots k})_+$ in general represents the spin function overlap from the integration region where the particle at x permutes to just behind x_j, while the particle at x' permutes to just behind x_k.

In general for arbitrary N, we obtain the spin-plus density matrix as

$$\rho_+(x < x') = N!\left\{ \int_{x<x'<x_2\cdots<x_N}(E,E)_+ + \int_{x<x_2<x'\cdots<x_N}(E,P_{12})_+ + \int_{x<x_2<x_3<x'\cdots<x_N}(E,P_{123})_+ + \cdots \right.$$
$$\left. + \int_{x_2<x<x'\cdots<x_N}(E,E)_+ + \int_{x_2<x<x_3<x'\cdots<x_N}(E,P_{12})_+ + \cdots + \int_{x_2<x_3\cdots<x_N<x<x'}(E,E)_+ \right\}$$
$$\times \psi_{\vec{n}}^{sym*}(x,\bar{x})\psi_{\vec{n}}^{sym}(x',\bar{x})d\bar{x}, \tag{10}$$

where we have used the properties of $(P_{12\ldots j}, P_{12\ldots j})_+ = (E,E)_+$ and $(E,P_{12\ldots j})_+ = (P_{12\ldots m}, P_{12\ldots m+j-1})_+$ for $j,m \geqslant 2$. The first property can be proved from Eq. (9) by using $P_{12\ldots j}^{-1} P_{12\ldots j} = E^{-1}E = 1$. To prove the second property, we can reduce $P_{12\ldots m}^{-1} P_{12\ldots m+j-1}$ to

$$(P_{m-1,m}\ldots P_{23}P_{12})^{-1}P_{m\ldots m+j-1}(P_{m-1,m}\ldots P_{23}P_{12})$$
$$= P_{12}^{-1}P_{23}^{-1}\ldots P_{m-1,m}^{-1}P_{m\ldots m+j-1}P_{m-1,m}\ldots P_{23}P_{12},$$
$$= P_{1,m+1\ldots m+j-1},$$

such that $(E, P_{1,m+1\ldots m+j-1})_+$, using again Eq. (9), is exactly the same as $(E,P_{12\ldots j})_+$.

Other spin components of the density matrices, $\rho_-(x < x')$ and $\rho_0(x < x')$, can be derived similarly from characterizing the respective normalized spin function overlaps $()_{-,0}$ which we will evaluate below.

From now on we limit ourselves to the specific sector of total $S_z \equiv \sum_{i=1}^N s_i = 0$. For S_z close to N, spin-1 Bose gas will behave not much different from the polarized or spinless one. Therefore, we choose the sector of zero S_z, which allows the SILL of spin-1 Bose gas to distinguish most significantly from the spinless bosons for $S_z \lesssim N$. The spin configurations $|\chi\rangle$ in this sector generally involve n pairs of $(+-)$, that is $|+++---00\ldots0\rangle$, with $n=3$ for example. The total number of states can then be calculated as

$$w_N \equiv \mathrm{Tr}_\chi(E) = \sum_{n=0}^{\frac{N}{2}\,\mathrm{or}\,\frac{N-1}{2}} \frac{N!}{(n!)^2(N-2n)!}, \tag{11}$$

which we obtain by permuting n $(\pm)$'s and $(N-2n)$ (0)'s. For the spin-plus component of the single-particle density matrix in Eq. (10), the spin configuration $|00\ldots0\rangle$ with $n=0$ never contributes. Therefore, we consider only the spin configurations of at least one pair of $(+-)$, and $|\chi\rangle$ can be generally expressed as

$$|+\underbrace{+\cdots+}_{n-1}\underbrace{-\cdots-}_{n}\underbrace{00\ldots0}_{N-2n}\rangle.$$

The first $+$ is projected out in $\rho_+(x < x')$, and thus we have the normalized spin function overlap $(E,E)_+$,

$$(E,E)_+ = \frac{1}{w_N}\sum_{n=1}^{\frac{N}{2}\,\mathrm{or}\,\frac{N-1}{2}} \frac{(N-1)!}{(n-1)!n!(N-2n)!}, \tag{12}$$

which is averaged by w_N, the total number of states. We note that all the arguments of the factorials should be equal and larger than zero. $(E,E)_+$ is proportional to the number of states obtained by permuting the rest of $(n-1)$ $(+)$'s, n $(-)$'s, and $(N-2n)$ (0)'s. For $(E,P_{12\ldots j})_+$, it has a contribution only when the first j entries are $(+)$'s,

$$|\underbrace{+\cdots+}_{j}\underbrace{+\cdots+}_{n-j}\underbrace{-\cdots-}_{n}\underbrace{00\ldots0}_{N-2n}\rangle,$$

such that we have

$$(E,P_{12\ldots j})_+ = \frac{1}{w_N}\sum_{n\geqslant j}^{\frac{N}{2}\,\mathrm{or}\,\frac{N-1}{2}} \frac{(N-j)!}{(N-2n)!n!(n-j)!}, \tag{13}$$

which denotes the number of states obtained by permuting the rest of $(n-j)$ $(+)$'s, n $(-)$'s, and $(N-2n)$ (0)'s. In this specific sector of zero S_z, we note that in general $(E,P_{12\ldots j})_+$ is nonvanishing only when $j \leqslant N/2$.

These corresponding spin function overlaps in $\rho_-(x < x')$, which are $(E,E)_-$ and $(E,P_{12\ldots j})_-$, should be the same as those in $\rho_+(x < x')$. For $\rho_0(x < x')$, we have the spin function overlaps as

$$(E,E)_0 = \frac{1}{w_N}\sum_{n=0}^{\frac{N}{2}\,\mathrm{or}\,\frac{N-1}{2}} \frac{(N-1)!}{(n!)^2(N-2n-1)!}, \tag{14}$$

$$(E,P_{12\ldots j})_0 = \frac{1}{w_N}\sum_{n=0}^{\frac{N}{2}\,\mathrm{or}\,\frac{N-1}{2}} \frac{(N-j)!}{(n!)^2(N-2n-j)!}, \tag{15}$$

which respectively denote the number of states contributed from the spin configurations with the first one and the first j
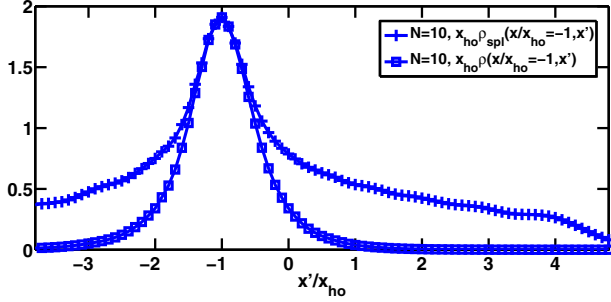
FIG. 1. Single-particle density matrix of spin-1 and spinless bosons for $N = 10$ in the sector of $S_z = 0$. The density matrix of spin-1 bosons is $\rho(x,x') = 2\rho_+(x,x') + \rho_0(x,x')$. The spatial correlations are plotted at chosen $x/x_{ho} = -1$. Spinless (spl) bosons (+) show broader spatial distributions than the spin-1 bosons ($\square$), indicating a narrower distribution in momentum space.

entries of (0)'s. We note of the identity that

$$2(E,E)_+ + (E,E)_0 = 1. \quad (16)$$

This also corresponds to the particle number conservation, that is $2N_+ + N_0 = N$, where $N_{\pm(0)} \equiv \int dx \, \rho_{\pm(0)}(x,x)$. Thus the number of particles is proportional to the spin function overlaps, $N_{\pm(0)} = N(E,E)_{\pm(0)}$. Furthermore, we note that

$$2(E,P_{12\ldots j})_+ + (E,P_{12\ldots j})_0 = w_{jN}/w_N, \quad (17)$$

where w_{jN} was defined in Ref. [27],

$$w_{jN} \equiv \sum_{n=0}^{\frac{N}{2} \text{ or } \frac{N-1}{2}} \left[\frac{(N-j)!}{(n!)^2(N-2n-j)!} + \frac{2(N-j)!}{(n-j)!n!(N-2n)!} \right]. \quad (18)$$

A. Spatial correlation in SILL of spin-1 Bose gas

The effect of the spin function overlaps in the SILL regime can be seen in Fig. 1 where we compare the spatial correlations of spin-1 [$\rho(x,x')$] and spinless bosons [$\rho_{spl}(x,x')$] at some chosen x in a harmonic trap. Spinless or spin-polarized bosons show a wider spatial distribution than the spin-1 case, indicating a sharper momentum distribution. Large $|x - x'|$ in the spatial correlation corresponds to the small p region. For spinless bosons, it has been shown in the bulk that $\rho_{spl,b}(x,x') \propto |x - x'|^{-1/2}$; thus small p behavior is proportional to $|p|^{-1/2}$ [42–45]. This narrow momentum distribution resembles the one of a Bose-Einstein condensate but not quite since no condensation is allowed [46] due to large quantum fluctuations in a 1D system. Therefore, no off-diagonal long-range order can be present in the density matrix of 1D Bose gas. However, a superfluid phase can exist in 1D quantum systems, possessing a power-law decay in spatial correlations. This power-law decay can be well described in the Luttinger liquid model using the bosonization method [17,18].

In a harmonic trap as shown in Fig. 1, the spatial correlations of $\rho_{spl}(x,x')$ are similar to the one in a bulk in a moderate region of $|x - x'|$ until the correlation decays faster at the edge of the trap ($x' \gtrsim 4x_{ho}$). In the trap, $\rho_{spl}(p = 0)$ is finite. It has also been shown that $\rho_{spl}(p = 0) \propto N$ in the large N limit [7].

In sharp contrast to the spinless bosons in Fig. 1, the spin-1 Bose gas in the SILL regime shows an exponential decay in its spatial correlation, which is therefore not condensed. This exponential decay has been predicted in the single-particle Green's function of quantum wires in the SILL regime [19,47,48], distinguishing from the Luttinger liquid with only power-law decays. In the momentum distributions, on the other hand, spin incoherence tends to broaden the distributions, which have been investigated in the $t - J$ model [24,49,50] or the system of uniform two-component gas [23]. Similarly, the spin-1 bosons in the SILL regime will also have a broadened momentum distribution due to the averaging of the spin function overlaps, which we discuss in more details below. Large p behavior will be discussed later in Sec. IV A.

B. Momentum distribution in SILL of spin-1 Bose gas

We define the spin-dependent momentum distributions as

$$\rho_{\pm(0)}(p) = \frac{1}{2\pi} \int_{-\infty}^{\infty} dx \int_{-\infty}^{\infty} dx' e^{ip(x-x')} \rho_{\pm(0)}(x,x'), \quad (19)$$

where we set $\hbar = 1$. We then numerically calculate the momentum distributions of the three components in 1D TG Bose gas based on Eq. (10), $\rho_-(x < x')$, and $\rho_0(x < x')$. In Fig. 2, both spin components of $\rho_+(p)$ and $\rho_0(p)$ are uniformly broadened as N grows, and $\rho_+(p) \neq \rho_0(p)$ for finite N. The effect of spin incoherence also averages out the oscillatory structure that is present in the momentum distribution for specific spin state of spinor Bose gas [11]. Furthermore, the peaks of $\rho_0(p)$ are larger than $\rho_+(p)$ up to $N = 16$. This is due to $N_0 \geqslant N_\pm$ in general and the spin function overlaps $(E,P_{12\ldots j})_0$ are always larger than $(E,P_{12\ldots j})_+$, which we will show more specifically in Fig. 9 in the Appendix. For spinless bosons, the peaks of $\rho_{spl}(p)$ have a scaling of $\rho_{spl}(p = 0) \propto N$ [7]. Here the spin-1 Bose gas in the SILL regime shows fitted scalings of $\rho_+(p = 0) \propto N^{0.49}$ and $\rho_0(p = 0) \propto N^{0.66}$ from Fig. 2. These reduced scalings again show the feature of broadened momentum distributions in the SILL regime

To calculate $\rho_{\pm(0)}(x,x')$ we implement Gaussian unitary ensemble (GUE) [7] to speed up the convergence in the Monte Carlo (MC) integration method. The GUE draws a series of $(N - 1)$ random numbers in $\bar{x}$, which are repulsively distributed due to the joint probability density of $\Pi_{1 \leqslant i < j \leqslant N-1}(x_i - x_j)^2$. This implementation of GUE thus enables our MC integration to simulate up to $N = 16$, which in this case takes about 140 h with MC simulations of $M = 10^6$ sets of random numbers using 200 parallel CPU cores. All MC simulations in Fig. 2 use $M = 10^7$ except for $N = 16$ with $M = 10^6$.

In the next section we investigate their asymptotic forms in large momentum limit, which show $1/p^4$ decay, and their momentum distributions in large N limit.

IV. MOMENTUM DISTRIBUTIONS IN HIGH p AND LARGE N LIMITS

A. Asymptotic high p limit

For spinless bosons in the TG limit, relative wave function between two particles in short distance is $\psi_{rel}(x,x') \propto |x - x'|$, indicating impenetrable bosons and corresponding to the
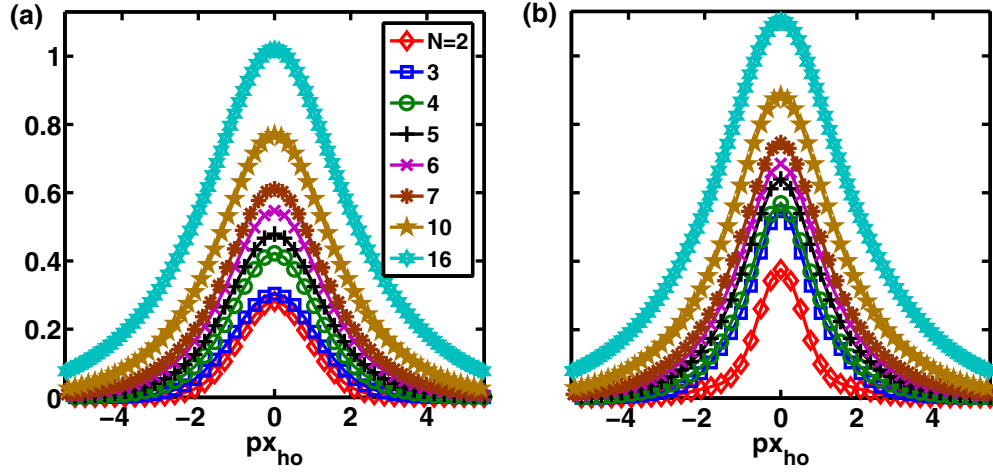
FIG. 2. Momentum distributions of (a) spin-plus $[\rho_+(p)]$ and (b) zero components $[\rho_0(p)]$ in the SILL regime. In the sector of $S_z = 0$, we numerically calculate the momentum distributions of 1D spin-1 TG gas up to $N = 16$. They are uniformly broadened as N increases, and the peaks of $\rho_0(p)$ are larger than $\rho_+(p)$ due to the spin function overlaps.

feature of fermionic repulsion. Again it has been shown [42–45] in a bulk where $\rho_{\mathrm{spl,b}}(x,x')$ in short distance is proportional to $[1 + \cdots + |x - x'|^3/(9\pi) + \cdots]$. Thus the nonanalytic $|x - x'|^3$ term in the short-distance correlation gives a universal $1/p^4$ asymptotic in large momentum limit. This universal $1/p^4$ asymptotic is not unique for a Bose gas with two-body contact interactions [8–10]. It also shows up in Tan's relation [51,52] in the two-component Fermi gas [53–56]. We note that the coefficient of the scaling depends on the many-body state and is related to the slope of energy $(-dE/dg_{\mathrm{1D}}^{-1})$ [9,22].

For 1D spin-1 TG Bose gas, on the other hand, the analytical results for a high p asymptotic total momentum distribution $\rho(p)$ have been derived [27], showing also a universal $1/p^4$ dependence. Similarly for its spin-dependent components, they can be straightforwardly written as

$$\rho_{\pm(0)}(p) \underset{p\to\infty}{=} \frac{2[(E,E)_{\pm(0)} + (E,P_{12})_{\pm(0)}]}{2\pi p^4}$$
$$\times \sum_{(n_i,n_j)} \int_{-\infty}^{\infty} dx \begin{vmatrix} \phi'_{n_i}(x) & \phi'_{n_j}(x) \\ \phi_{n_i}(x) & \phi_{n_j}(x) \end{vmatrix}^2, \quad (20)$$

where (n_i, n_j) denotes any possible pairs of N harmonic-oscillator eigenfunctions. The asymptotic form depends on the spin function overlap $(E,P_{12})_{\pm(0)}$ because it has significant contributions only from the integral regions of $x < x_j < x'$ and $x' < x_j < x$ for all $x_j \in \bar{x}$ with $x \approx x'$. The asymptotic form for the spinless bosons can be also obtained by replacing $[(E,E)_{\pm(0)} + (E,P_{12})_{\pm(0)}]$ with 2 in Eq. (20). We note that, using Eqs. (20) and (18), we have $2\rho_+(p) + \rho_0(p) = \rho(p)$ where the last quantity was computed in Ref. [27].

The spin-1 Bose gas in the SILL regime shows very different properties from the spin-coherent ones in the coefficients of high p asymptotics. The coefficients are always less than the ones in spinless bosons since $(E,E)_{\pm(0)}, (E,P_{12})_{\pm(0)} < 1$. This is because the spin part of the wave function is no longer necessarily symmetric under interchange of two particles. And for large N, $[(E,E)_{\pm(0)} + (E,P_{12})_{\pm(0)}] \to [1/3 + (1/3)^2] = 4/9$

from Eq. (A22), less than 2 for the case of spinless bosons as well. As an example, in Fig. 3 we compare the numerical and analytical results of $\rho_+(p)$ in high p limit. The numerically calculated high p asymptotics approach approximately the analytical ones. For even larger $px_{ho} \gtrsim 7$, the trends either drop and cross the analytical asymptotics, or bounce back and oscillate, indicating the inaccuracy of numerical results in these regions. To reach accurate high p asymptotics is quite demanding in MC integrations and consuming more CPU time for even larger N. However, MC simulations have already achieved the accuracy of 10^{-3} and 10^{-2} of the momentum distributions for $N = 2$–3 and 10, respectively.

We have also evaluated numerically the potential $(\langle V \rangle)$ and kinetic energies $(\langle K \rangle)$. Since our 1D bosonic TG gas has the same density distribution as the one of a Fermi gas, we have $\langle V \rangle = \langle K \rangle = N^2\hbar\omega/4$, equivalent to half of the total energy, which complies with the virial theorem [57,58]. In Ref. [27], we concatenate $\rho(p)$ with the asymptotic tails
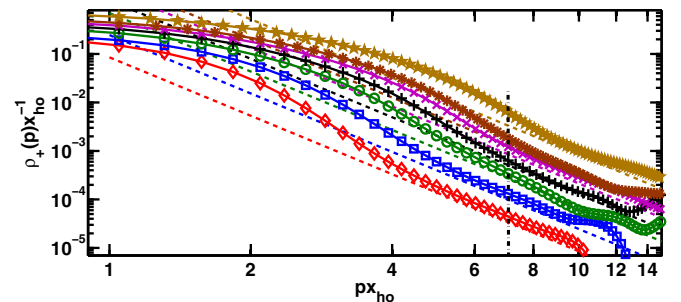

FIG. 3. Asymptotics of high momentum distributions in Fig. 2. High momentum distributions are plotted in logarithmic scales and compared with analytic calculations (dash) in the spin-plus component of 1D spin-1 TG Bose gas. The analytical asymptotics are $(0.085, 0.245, 0.694, 1.267, 2.131, 3.225, 8.305)/p^4$, respectively for $N = 2$–7 and 10. The line symbols and colors are the same as Fig. 2, and a vertical line (dash-dot) at around $px_{ho} \sim 7$ guides the eye for the limitation in accuracy of the numerical calculations.
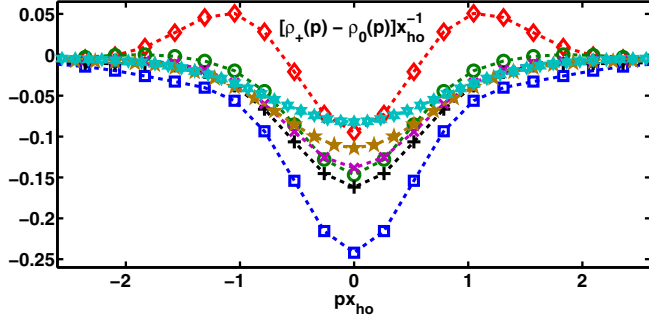
FIG. 4. Difference between spin-plus and spin-zero momentum distributions. The symbols and colors are plotted correspondingly as in Fig. 2, where we choose $N = 2$–6 and 16. The case of $N = 7$ is neglected here for it is too close to the one of $N = 6$. The difference diminishes gradually as N increases.

analytically derived to improve the energy calculations. Here we directly use the momentum distributions of $\rho(p)$ calculated by MC simulations implemented with GUE. We find that the numerical results of these energies improve to the relative errors below 7% and 10% for $N = 2$–7 and 16 respectively to the exact values of $\langle V \rangle$ and $\langle K \rangle$. This further shows the advantage of GUE in the convergence and accuracy of our numerical results.

In Fig. 4, we plot the difference of spin-plus and zero momentum distributions numerically, $\rho_+(p) - \rho_0(p)$, from Fig. 2. The difference goes away gradually as N increases, indicating these two components approach each other in large N limit. The dips at around $p \sim 0$ demonstrate that the peaks of $\rho_0(p)$ are always higher than $\rho_+(p)$, which is due to larger spin function overlaps for the spin-zero component. A special feature of the peaks for the case of $N = 2$ shows a wider $\rho_+(p)$ than $\rho_0(p)$, while this feature is not obvious for larger N.

B. Large N limit

Due to the limits of numerical integration, we can only calculate the single-particle density matrix of spin-1 bosons up to $N = 16$. For finite N, we have demonstrated numerically $\rho_+(p) \neq \rho_0(p)$ since in general $N_0 \geqslant N_+$ and spin function overlaps $(E, P_{12\ldots j})_0$ are always larger than $(E, P_{12\ldots j})_+$. Thus the peaks of $\rho_0(p = 0)$ are larger than $\rho_+(p = 0)$. In this subsection we attempt to investigate the momentum distributions in large N limit. The study in this limit can give insight to practical experiments where several hundreds or thousands of atoms are involved.

To investigate the individual components of spin-1 momentum distributions in large N limit, we need the asymptotic forms for various spin function overlaps. These spin function overlaps in general can be written as

$$(E, E)_+ = \frac{f_1^{(N-1)}}{f_0^{(N)}}, \quad (E, P_{12\ldots j})_+ = \frac{f_j^{(N-j)}}{f_0^{(N)}},$$

$$(E, E)_0 = \frac{f_0^{(N-1)}}{f_0^{(N)}}, \quad (E, P_{12\ldots j})_0 = \frac{f_0^{(N-j)}}{f_0^{(N)}}, \quad (21)$$
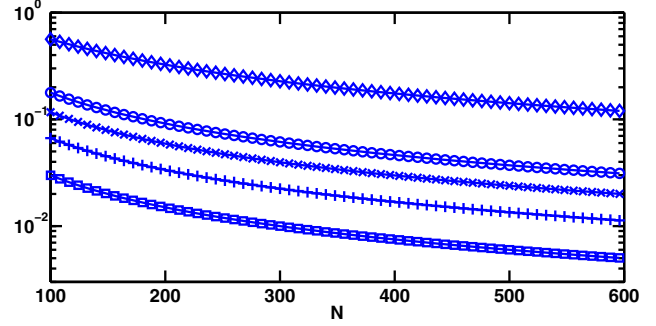

FIG. 5. Relative deviations of Eq. (24) for the asymptotic forms $\bar{f}_j^{(N-j)}$ and $\bar{f}_0^{(N-j)}$ of the exact spin function overlaps $(E, P_{12\ldots j})_+$ and $(E, P_{12\ldots j})_0$, respectively. The relative deviations are plotted for $j = 2(\square)$, $3(+)$, $4(\times)$, $5(\circ)$, and $10(\diamond)$. The deviations decrease as N increases, which indicates that the asymptotic forms are approaching each other. It suggests that spin-plus and zero components of the momentum distributions coincide in the large N limit.

where

$$f_k^{(N)} \equiv \sum_{j=0}^{\frac{N-k}{2}} \frac{N!}{(k+j)! \, j! \, (N-2j-k)!}. \quad (22)$$

We find the asymptotic form of $f_k^{(N)}$ in large N limit in the Appendix using the method of steepest descent or stationary phase [59]. In Fig. 9 of the Appendix, the asymptotic forms in Eq. (A20) are used to compare with the exact ones of Eqs. (12), (13), (14), and (15), and they approach the exact ones in large N limit for small j in Eq. (21). Therefore, we shall use the asymptotic forms to compare the spin-plus with the spin-zero components of the spin function overlaps for large N.

We define their relative deviations as

$$\left| \frac{(E, P_{12\ldots j})_+ - (E, P_{12\ldots j})_0}{(E, P_{12\ldots j})_0} \right|, \quad (23)$$

which asymptotically approaches to

$$\left| \frac{\bar{f}_j^{(N-j)} - \bar{f}_0^{(N-j)}}{\bar{f}_0^{(N-j)}} \right|, \quad (24)$$

in large N limit, where $\bar{f}_j^{(N-j)}$ is the asymptotic form of $f_j^{(N-j)}$. This asymptotic form allows us to compute the deviations for even larger N than using the exact formulas. In Fig. 5, the relative deviations decay as N increases for small j and become below 10^{-2} for $N \sim 600$ with $j \leqslant 3$. Note that for a moderate $j = 10$, it only reaches 0.1 for as high as $N = 600$. Since the spin function overlaps with smaller j contribute much more to the momentum distributions than $j \lesssim N/2$ [see Figs. 9(a) and 9(b)], along with much less relative deviations, we expect that the spin-plus momentum distribution approaches the one of spin-zero as N increases. We have also shown this trend in Fig. 4 for finite N up to sixteen particles.

This can be further confirmed by studying respective contributions from the integral regions in the single-particle density matrix $\rho_+(x < x')$ of Eq. (10). In Fig. 6 we plot the results of most significant 12 out of a total 15 integral regions
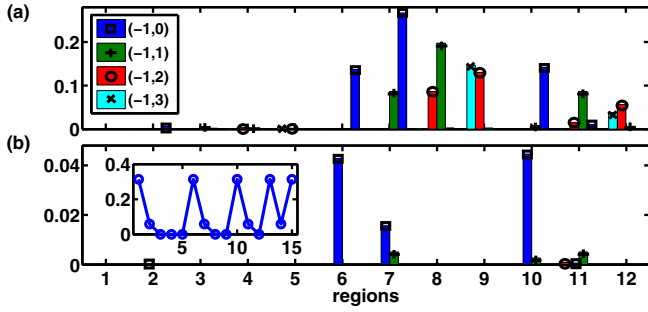
FIG. 6. Contributions from the integral regions for $\rho_+(x < x')$ with $N = 5$. The values for each integral region without and with the multiplications of spin function overlaps are shown in (a) and (b), respectively. Four spatial correlations are chosen at (x,x') as denoted in the legend of (a) along with the symbols ($\square, +, \circ, \times$) for clarity. The inset in (b) displays 15 spin function overlaps for the case of five bosons.

for the case of $N = 5$ with and without the multiplications of spin function overlaps. The order of the integral regions can be seen from Eq. (10). We denote the first five regions as $x < x_2$ with $x' < x_2$ moving sequentially to $x_5 < x'$, the next four regions (sixth to tenth) as $x_2 < x < x_3$ with $x_2 < x' < x_3$ moving sequentially to $x_5 < x'$, and so on for the rest of the regions. A feature of hard core bosons in 1D harmonic trap is that atoms prefer to distribute evenly in space. The particles at $\bar{x}$ repel each other due to their strongly repulsive interactions in TG limit. Thus more significant peaks of the integral contributions occur roughly at the corresponding integral regions depending on (x,x'). For example, in Fig. 6(a), the spatial correlation at $(x,x') = (-1,0)$ has the largest contribution at the seventh integral region, $x_2 < x < x_3 < x' < x_4 < x_5$. Similarly the spatial correlation at $(x,x') = (-1,3)$ has the largest contribution at the ninth integral region, $x_2 < x < x_3 < x_4 < x_5 < x'$. In Fig. 6(b) we multiply these values with the spin function overlaps (inset), and show that significant contributions come from the overlaps with small j. For four specific spatial correlations we choose here, significant values dwell in the sixth, seventh, tenth, and eleventh integral regions, which correspond to the spin function overlaps $(E,E)_+$, $(E,P_{12})_+$, $(E,E)_+$, and $(E,P_{12})_+$, respectively. Moreover, as expected, the spatial correlations decay as $|x - x'|$ increases, reminiscent of the exponential decay discussed in Sec. III A.

For TG bosons in the bulk with a length L in thermodynamic limit, we can use the analytical expression of Eq. (20) and let $\phi_{n_i}(x) = e^{ik_ix}/\sqrt{L}$ with various eigenmodes $n_i \to k_i$. The spatial integral in Eq. (20) can then be calculated as

$$\int dx \begin{vmatrix} \phi'_{n_i}(x) & \phi'_{n_j}(x) \\ \phi_{n_i}(x) & \phi_{n_j}(x) \end{vmatrix}^2$$

$$= \frac{1}{L^2} \int dx \begin{vmatrix} ik_i e^{ik_ix} & ik_j e^{ik_jx} \\ e^{ik_ix} & e^{ik_jx} \end{vmatrix}^2$$

$$= \frac{(k_i - k_j)^2}{L}. \tag{25}$$

In the continuous limit of (k_i,k_j) corresponding to the pairs of (n_i,n_j) in the summation, we have $\rho_{\rm spl,b}(p \to \infty)$ in the bulk

$$\frac{\rho_{\rm spl,b}(p \to \infty)}{L} = \frac{2}{\pi p^4} \int_{-k_F}^{k_F} \frac{dk_i}{2\pi} \int_{-k_F}^{k_i} \frac{dk_j}{2\pi} (k_i - k_j)^2, \tag{26}$$

where $k_F = \pi N/L$. Letting $k_i = k_F x$ and $k_j = k_F y$, the above becomes

$$\frac{\rho_{\rm spl,b}(p \to \infty)}{L} = \frac{k_F^4}{2\pi^3 p^4} \int_{-1}^{1} dx \int_{-1}^{x} dy (x - y)^2$$

$$= \frac{2k_F^4}{3\pi^3 p^4}, \tag{27}$$

which is the same as Eq. (67) in Ref. [45] up to a factor of 2π in our definition of Fourier transform in Eq. (19). Our derivation is parallel to using short-distance expansions in $\rho_{\rm spl,b}(x,x')$ [45], where its nonanalytic term $|x - x'|^3/(9\pi)$ after Fourier transform gives the same result.

For large N spinless bosons in a harmonic trap, we can use the local-density approximation (LDA) for the local chemical potential in Thomas-Fermi limit, which reads $\mu(x) = \mu - \alpha x^2/2$ with $\alpha = M\omega^2$. The cutoff momentum can be derived as $k_F(x) = \sqrt{2M(\mu - \alpha x^2/2)}$. Since the maximum mode in 1D hard core bosons at infinite interactions is approximately $n_{\rm max} \approx N$, the chemical potential can be determined as $\mu = n_{\rm max}\omega \approx N\omega$. We further define the boundary of $x_{\rm max} = \sqrt{2N\omega/\alpha}$ such that we reexpress $k_F(x)$ as $\sqrt{(M\alpha)(x_{\rm max}^2 - x^2)}$. Applying LDA to Eq. (27), we have the density matrix for spinless bosons in a harmonic trap as

$$\rho_{\rm spl,LDA}(p \to \infty) = \frac{2}{3\pi^3} \int_{-x_{\rm max}}^{x_{\rm max}} dx \frac{k_F^4(x)}{p^4}$$

$$= \frac{2(M\alpha)^2}{3\pi^3 p^4} \int_{-x_{\rm max}}^{x_{\rm max}} dx (x_{\rm max}^2 - x^2)^2$$

$$= \frac{2^7\sqrt{2}}{45\pi^3} N^{5/2} \frac{1}{p^4 x_{ho}^3}, \tag{28}$$

where the scaling of $N^{5/2}$ disagrees with Ref. [9], which gave a different scaling of $N^{3/2}$. $N^{5/2}$ scaling has also been reported for the 1D SU(κ) Fermi gas with $\kappa \neq 1$ [22]. The coefficient in Eq. (28) is the same as the TG Fermi gas in the $\kappa \to \infty$ limit.

For the spinful case of our spin-1 Bose gas in large N limit, the asymptotic coefficient of $[(E,E)_{\pm(0)} + (E,P_{12})_{\pm(0)}]$ becomes $[1/3 + (1/3)^2] = 4/9$ according to Eq. (A22), such that the spin-dependent and total momentum distributions respectively in thermodynamic limit become

$$\rho_{\pm(0)}(p \to \infty)|_{N\to\infty} = \frac{1}{2}\frac{4}{9}\rho_{\rm spl,LDA}(p \to \infty)$$

$$= \frac{2^8\sqrt{2}}{405\pi^3} N^{5/2} \frac{1}{p^4 x_{ho}^3} \tag{29}$$
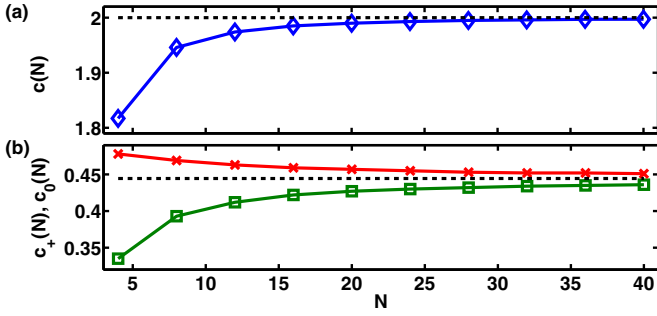
FIG. 7. Comparisons of the coefficients in the momentum distributions of spinless and spin-1 Bose gas. We plot the coefficients of (a) $c(N)$ ($\diamond$) and (b) $c_+(N)$ ($\square$) and $c_0(N)$ ($\times$), respectively for spinless bosons, spin-plus, and spin-zero components in high p limit. These coefficients approach the asymptotic values $c(\infty) = 2$ (dash) and $c_{+(0)}(\infty) = 4/9$ (dash) when N increases.

and

$$\rho(p \to \infty)|_{N \to \infty} = 3\rho_{\pm(0)}(p \to \infty)|_{N \to \infty}$$
$$= \frac{2^8 \sqrt{2}}{135\pi^3} N^{5/2} \frac{1}{p^4 x_{ho}^3}, \quad (30)$$

which is 2/3 of Eq. (28).

We denote the momentum distribution of spinless bosons in high p limit as $\rho_{spl}(p \to \infty)$ which can be derived by replacing $[(E,E)_{\pm(0)} + (E,P_{12})_{\pm(0)}]$ with 2 in Eq. (20). We then define $c(N) \equiv \rho_{spl}(\infty)(2^6\sqrt{2})^{-1}N^{-5/2}(45\pi^3 p^4 x_{ho}^3)$ and $c(\infty) = 2$ according to Eq. (28). $c_{\pm(0)}(N)$ can be also defined in the same way for $\rho_{\pm(0)}(\infty)$. These coefficients can be calculated using Eq. (20). In Fig. 7 we plot $c(N)$ and $c_{+(0)}(N)$ respectively to show how they approach the asymptotic large N values. We find that Eqs. (28) and (29) already give good enough estimates for $N \gtrsim 20$ and 30 for spinless and spin-1 bosons, respectively. The relative deviations $|c(N) - c(\infty)|/c(\infty) = 0.14\%$ for $N = 40$, and for the cases of $c_{+(0)}(40)$, they reach $1.9\%(1.5\%)$. In Fig. 7(b), $c_0 > c_+$, which again indicates that the spin function overlaps $(E,P_{12\ldots j})_0 > (E,P_{12\ldots j})_+$ and $N_0 > N_+$.

V. CONCLUSION

In conclusion, we have investigated the spin-dependent properties of spin-1 Bose gas in the regime of spin-incoherent Luttinger liquid (SILL). Three components (spin-plus, zero, and minus) of the single-particle density matrix for this universal class can be calculated by deriving respective spin function overlaps. These spin function overlaps result from the highly degenerate spin configurations in the SILL regime. In contrast with the spinless bosons with a power-law decay in its spatial correlation, spin-1 bosons in TG limit show an exponentially decaying spatial correlation, which indicates a broadened momentum distribution and a different universal class from Luttinger liquid. The universal $1/p^4$ dependence in high p limit is also present in the spin-dependent momentum distributions. This asymptotic has a scaling of $N^{5/2}$ with a reduced coefficient than the one of the spinless bosons. The coefficients of the asymptotic are proportional to Tan's

contact and can be observed in experiments as one of the signatures of SILL. We compare these analytical predictions with the numerical results calculated by Monte Carlo (MC) integration with Gaussian unitary ensemble (GUE) up to sixteen bosons. The method of MC integration implemented with GUE converges faster and gives more accurate results such that we are able to calculate higher p regions. The high momentum tails approximately and asymptotically follow the reduced coefficients we analytically derived.

For the $S_z = 0$ sector, we show that the spin-zero component always has a larger peak than the spin-plus momentum distribution for finite N. This can be explained by the spin function overlaps which are larger for the spin-zero density matrix than the spin-plus case. While they differ for small N, they coincide in the large N limit. This indicates that highly incoherent bosons form in this limit with each component occupying exactly one-third of the total number of particles. The ultracold spinor Bose gas allows for a potential realization of this universal class of SILL, and our results offer a testable paradigm to study quantum many-body phenomena in 1D strongly interacting bosons.

APPENDIX: SPIN FUNCTION OVERLAPS IN LARGE N LIMIT

Before we derive the spin function overlaps in large N limit, first we express them in terms of an integral function, and then introduce the method of stationary phase or steepest descent to solve for their asymptotic forms [59]. Consider the following function:

$$f^{(N)}(x) = (x + x^{-1} + 1)^N$$
$$= \sum_{j_2=0}^{N} \sum_{j_1=0}^{N-j_2} \frac{N!}{j_1! j_2! (N - j_1 - j_2)!} x^{j_1 - j_2}, \quad (A1)$$

where the second line above can be derived by binomial expansions. When we set $k = j_1 - j_2$ and $j = j_2$, we have

$$f^{(N)}(x) = \sum_{k=-N}^{N} \sum_{j=0}^{\frac{N-k}{2}} \frac{N!}{(k+j)! j! (N - 2j - k)!} x^k, \quad (A2)$$

where the upper bound of index j can be derived by solving j_2 in the equations of $j_1 + j_2 = N$ and $j_1 - j_2 = k$. From Eq. (A2), we define the coefficient of x^k in $f^{(N)}(x)$ as $f_k^{(N)}$ which is the same as the one of x^{-k}. $f_k^{(N)}$ is defined in Eq. (22) in the main paper. Comparing with Eqs. (12), (13), (14), and (15) in the main paper, we find that the spin function overlaps can be expressed as Eq. (21) in the main text. These coefficients
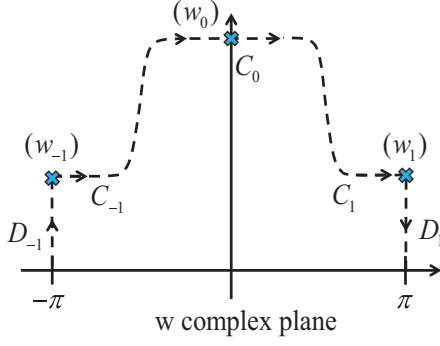
FIG. 8. Integration paths for calculating the asymptotic form of $f_k^{(N)}$ traversing through three saddle points (denoted as ×). Starting from $w = -\pi$ in the complex plane of w, we choose a vertical path D_{-1} to reach the first saddle w_{-1} with increasing imaginary parts only. Paths $C_{\pm 1}$ traverse through the saddle points $w_{\pm 1}$ from the left tangent to the real axis, which connect to the path C_0 crossing the third one w_0, again tangent to the real axis. The last path D_1 reaches the end point of $w = \pi$ starting from w_1. Paths $C_{\pm 1}$ and C_0 follow the valleys of steepest descent while $D_{\pm 1}$ do not.

can be calculated as follows:

$$f_k^{(N)} = \frac{1}{2\pi i} \oint_C dz \, z^{k-1} (z + z^{-1} + 1)^N, \qquad (A3)$$

where the coefficient $f_k^{(N)}$ (of z^{-k} in this case) is exactly the residue at the pole of $z = 0$ with a complex number z. C in the above denotes a contour integration on a circle in a counterclockwise direction around the origin.

The asymptotic behavior of the integral can be obtained in large N limit. We let $z = e^{i\theta}$; the coefficient becomes

$$
\begin{aligned}
f_k^{(N)} &= \frac{1}{2\pi} \int_{-\pi}^{\pi} d\theta \, e^{ik\theta} (1 + 2\cos\theta)^N \\
&= \frac{1}{2\pi} \int_{-\pi}^{\pi} d\theta \, e^{\mathcal{F}(\theta)}, \qquad (A4)
\end{aligned}
$$

where $\mathcal{F}(\theta) \equiv N \ln(1 + 2\cos\theta) + ik\theta$. Let $\theta \to w$ in the complex plane, using the method of steepest descent [59] for the above highly oscillating integrals in large N limit, we first find the saddle points which satisfy the first derivative $\mathcal{F}'(w) = 0$. The integrals are then dominated by the local maxima passing the saddle points along the integration contour.

The saddle points are therefore located at

$$-2\sin w + \frac{ik}{N}(1 + 2\cos w) = 0, \qquad (A5)$$

which, after replacing trigonometry functions with exponentials, becomes

$$e^{iw} = \frac{-k/N \pm \sqrt{(k/N)^2 + 4(1 - k^2/N^2)}}{2(1 + k/N)}. \qquad (A6)$$

If $k \to 0$, the above suggests a multiple of roots that satisfy $e^{iw} = \pm 1$, which are $w = 2n\pi$ and $\pm(2n+1)\pi$ for integers n, indicating multiple saddle points in this integral. We consider an integration path in Fig. 8, where only three saddle points ($n = 0$) are involved. Below we demonstrate why the contour is valid and guarantees to follow the valleys of steepest descent

between these three saddle points, which can be determined by the sign of $\mathcal{F}''(w)$.

First to calculate $\mathcal{F}''(w_0)$, we define $Q \equiv \sqrt{4 - 3(k/N)^2}$, and we have from Eq. (A6) with the "+" sign,

$$e^{iw_0} = \frac{-k/N + Q}{2(1 + k/N)}, \quad e^{-iw_0} = \frac{k/N + Q}{2(1 - k/N)}, \qquad (A7)$$

where w_0 should be purely imaginary in general. We further use the above to reinterpret

$$
\begin{aligned}
\cos w_0 &= \frac{(k/N)^2 + Q}{2[1 - (k/N)^2]}, \quad 1 + 2\cos w_0 = \frac{1 + Q}{1 - (k/N)^2}, \\
\sin w_0 &= \frac{i}{2} \frac{k}{N} \frac{1 + Q}{1 - (k/N)^2}. \qquad (A8)
\end{aligned}
$$

Now the second derivative of $\mathcal{F}(w_0)$ becomes

$$
\begin{aligned}
\mathcal{F}''(w_0) &= N\left[\frac{-2\cos w_0}{1 + 2\cos w_0} - \frac{4\sin^2 w_0}{(1 + 2\cos w_0)^2} \right] \\
&= -N \frac{[Q(1 - (k/N)^2)]}{1 + Q}, \qquad (A9)
\end{aligned}
$$

which is always less than zero. For example, $\mathcal{F}''(w_0) = -2N/3$ and $-N\epsilon$ respectively at small and large k limit ($k/N = 1 - \epsilon$ with $\epsilon \gtrsim 0$).

Next for $\mathcal{F}''(w_{\pm 1})$ at the other two saddle points which we denote as $w_{\pm 1}$, we have from Eq. (A6) with the "−" sign,

$$e^{iw_{\pm 1}} = \frac{-k/N - Q}{2(1 + k/N)}, \quad e^{-iw_{\pm 1}} = \frac{k/N - Q}{2(1 - k/N)}, \quad (A10)$$

where $w_{\pm 1}$ in general are complex. Setting $w_{\pm 1} = \pm\pi + iy_1$ with real y_1, we have $e^{-y_1} \lesssim 1$ and $e^{-y_1} \approx 1/2$ respectively when $k \to 0$ and $k \to N$, suggesting $y_1 \gtrsim 0$ at small k limit. Again we can use the above to reinterpret

$$
\begin{aligned}
\cos w_{\pm 1} &= \frac{(k/N)^2 - Q}{2[1 - (k/N)^2]}, \quad 1 + 2\cos w_{\pm 1} = \frac{1 - Q}{1 - (k/N)^2}, \\
\sin w_{\pm 1} &= \frac{i}{2} \frac{k}{N} \frac{1 - Q}{1 - (k/N)^2}. \qquad (A11)
\end{aligned}
$$

Now the second derivative of $\mathcal{F}(w_{\pm 1})$ becomes

$$\mathcal{F}''(w_{\pm 1}) = -N \frac{Q[1 - (k/N)^2]}{Q - 1}, \qquad (A12)$$

which is again always less than zero, for example, $\mathcal{F}''(w_0) = -2N$ and $-2N/3$ respectively for small and large k limit.

Now we have located three saddle points, which are w_0 and $w_{\pm 1}$. The asymptotic form of the integral for $f_k^{(N)}$ in Eq. (A4) can then be calculated using the contour in Fig. 8, which traverses through these three saddle points on the paths tangent to the real axis. Following the integration contour for Eq. (A4), we have the asymptotic form $\bar{f}_k^{(N)}$ of $f_k^{(N)}$ as

$$\bar{f}_k^{(N)} = \frac{1}{2\pi} \left[\int_{D_{-1}} + \int_{C_{-1}} + \int_{C_0} + \int_{C_1} + \int_{D_1} \right] d\theta \, e^{\mathcal{F}(\theta)}. \qquad (A13)$$

We obtain the contributions of w_0 in the path C_0 as

$$\frac{1}{2\pi}\int_{C_0} dw\, e^{\mathcal{F}(w_0)} e^{\frac{1}{2}\mathcal{F}''(w_0)(w-w_0)^2}$$

$$= \frac{e^{\mathcal{F}(w_0)}}{2\pi}\int_{C_0} dw\, e^{-\frac{1}{2}|\mathcal{F}''(w_0)|(w-w_0)^2}$$

$$= \frac{e^{\mathcal{F}(w_0)}}{2\sqrt{\pi}\sqrt{-\mathcal{F}''(w_0)/2}}, \tag{A14}$$

where its next correction term is at least $O(N^{-1/2})$ smaller. Since the integration path $C_{0(\pm 1)}$ follows the valley of steepest descent, the integration is dominated near the region of the saddle point $w_{0(\pm 1)}$, where we are also able to allow the boundary of w to $\pm\infty$. Similarly for the paths $C_{\pm 1}$, we have the contributions from $w_{\pm 1}$,

$$\frac{e^{\mathcal{F}(w_1)}}{2\pi}\left[\int_{C_{-1}} dw\, e^{\frac{1}{2}\mathcal{F}''(w_{-1})(w-w_{-1})^2} + \int_{C_1} dw\, e^{\frac{1}{2}\mathcal{F}''(w_1)(w-w_1)^2}\right], \tag{A15}$$

where $\mathcal{F}(w_{-1}) = \mathcal{F}(w_1)$. Letting $w = w_{\pm 1} + x$ in the paths $C_{\pm 1}$, respectively, we have

$$\frac{e^{\mathcal{F}(w_1)}}{2\pi}\left[\int_0^\infty dx\, e^{-\frac{1}{2}|\mathcal{F}''(w_{-1})|x^2} + \int_{-\infty}^0 dx\, e^{-\frac{1}{2}|\mathcal{F}''(w_1)|x^2}\right]$$

$$= \frac{e^{\mathcal{F}(w_1)}}{2\pi}\int_{-\infty}^\infty dx\, e^{-\frac{1}{2}|\mathcal{F}''(w_1)|x^2}$$

$$= \frac{e^{\mathcal{F}(w_1)}}{2\sqrt{\pi}\sqrt{-\mathcal{F}''(w_1)/2}}, \tag{A16}$$

where we have used $\mathcal{F}''(w_{-1}) = \mathcal{F}''(w_1)$. For the paths of $D_{\pm 1}$, though they do not follow the valleys of steepest descent, their contributions cancel with each other since $\mathcal{F}(w) = \mathcal{F}(w + 2\pi)$.

Finally we obtain the asymptotic form of $f_k^{(N)}$ in large N limit as

$$\bar{f}_k^{(N)} = \frac{1}{2\sqrt{\pi}}\left[\frac{e^{\mathcal{F}(w_0)}}{\sqrt{-\mathcal{F}''(w_0)/2}} + \frac{e^{\mathcal{F}(w_1)}}{\sqrt{-\mathcal{F}''(w_1)/2}}\right]. \tag{A17}$$

Before we write down the explicit form for the above, it is useful to derive

$$e^{\mathcal{F}(w_0)} = \left[\frac{1+Q}{1-(k/N)^2}\right]^N \left[\frac{Q-k/N}{2(1+k/N)}\right]^k, \tag{A18}$$

which become 3^N and $1/\epsilon^{N\epsilon}$ respectively for small and large k. Also we have

$$e^{\mathcal{F}(w_{\pm 1})} = (-1)^{N+k}\left[\frac{Q-1}{1-(k/N)^2}\right]^N \left[\frac{Q+k/N}{2(1+k/N)}\right]^k, \tag{A19}$$

which become $(-1)^{N+k}$ and $(3/4)^N 2^{N\epsilon}/(-1)^{N\epsilon}$ respectively for small and large k. Inserting the functions of the saddle
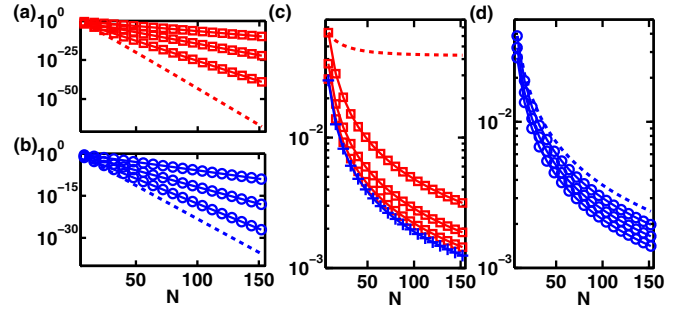

FIG. 9. Exact spin function overlaps and their relative deviations from analytical derivations. Exact spin function overlaps, $(E, P_{12\ldots j})_{+,0}$, for spin-plus and spin-zero components are plotted in (a) and (b) respectively, top to bottom, from $j/N = 1/8$, $2/8$, and $3/8$ (solid) to $j = N/2 - 1$ (dash). The values decrease rapidly as j increases. The relative deviations of the exact spin function overlaps $(E, P_{12\ldots j})_{+,0}$ from $\bar{f}_{j,0}^{(N-j)}/\bar{f}_0^{(N)}$ are plotted for $j = 1/8$, $2/8$, and $3/8$ (solid-□ and ○), and $j = N/2 - 1$ (dash), bottom to top, in (c) and (d), respectively. The deviations increase as j increases. The relative deviations of $(E, E)_{+,0}$ from $\bar{f}_{1,0}^{(N-1)}/\bar{f}_0^{(N)}$ are denoted as $(+)$ in (c), which almost overlap with each other. $(E, E)_{+(0)}$ reaches $0.333(0.334)$ at $N = 150$ and should approach $1/3$ for even larger N as indicated by Eq. (A22).

points from Eqs. (A9), (A12), (A18), and (A19), we have

$$\bar{f}_k^{(N)} = \left[(1+Q)^{N+\frac{1}{2}}\left(Q-\frac{k}{N}\right)^k \right. $$
$$\left. + (-1)^{N+k}(Q-1)^{N+\frac{1}{2}}\left(Q+\frac{k}{N}\right)^k\right]$$
$$\times \frac{\left[2\left(1+\frac{k}{N}\right)\right]^{-k}}{\sqrt{2NQ\pi}\left[1-\left(\frac{k}{N}\right)^2\right]^{N+\frac{1}{2}}}. \tag{A20}$$

We note that the main contribution in Eq. (A20) comes from the saddle point w_0. To have some estimates of Eq. (A20), we have

$$\bar{f}_{k\to 0}^{(N)} = \frac{3^N}{2\sqrt{\pi}\sqrt{N/3}}, \quad \bar{f}_{k\to N}^{(N)} = \frac{1}{\sqrt{2\pi N\epsilon}\cdot\epsilon^{N\epsilon}}. \tag{A21}$$

From the above result at small k and according to Eq. (21), we can show that

$$\left.\frac{(E, P_{12\ldots j+1})_{+(0)}}{(E, P_{12\ldots j})_{+(0)}}\right|_{N\to\infty} = \frac{1}{3},$$

$$(E, E)_+\big|_{N\to\infty} = (E, E)_0\big|_{N\to\infty} = \frac{1}{3}, \tag{A22}$$

which respectively indicates one-third decrease for the spin function overlaps when j increases by one, and the populations of N_+ and N_0 coincide in large N limit. In the large N limit, despite the constraint $S_z = 0$, the probability of finding a particle in any of the spin states, $+$, zero, or $-$, is $1/3$ and is irrespective of the spins of the other particles (if $j \ll N$). This decrease in spin function overlaps also reflects on the exponential decay in spatial correlations discussed in Sec. III A.

To have some estimates of the spin function overlaps and their asymptotic forms in large N limit, in Fig. 9 we

compare $(E,P_{12...j})_{+,0}$ of Eqs. (13) and (15) with $\bar{f}_{j,0}^{(N-j)}/\bar{f}_0^{(N)}$ from Eq. (A20). In Figs. 9(a) and 9(b), the values of spin function overlaps decrease rather fast in logarithmic scales as j increases, while $(E,P_{12...j})_0$ is always larger than $(E,P_{12...j})_+$. As a comparison, we define the relative deviations as

$$\left| \frac{(E,P_{12...j})_{+,0} - \bar{f}_{j,0}^{(N-j)}/\bar{f}_0^{(N)}}{(E,P_{12...j})_{+,0}} \right|, \qquad \text{(A23)}$$

which we show in Figs. 9(c) and 9(d), indicating a good asymptotic form from our derivations for small j in large N limit. However, a slow decay in the relative deviation of $(E,P_{12...N/2-1})_+$ to $\bar{f}_{N/2-1}^{(N/2+1)}/\bar{f}_0^{(N)}$ in Fig. 9(c) shows the worst case in the asymptotic form. It is due to a rather small $\mathcal{F}''(w_0) \to -N\epsilon$ in Eq. (A9) when we set $k/N = 1 - \epsilon$ with a small value of ϵ, which makes the method of steepest descent less accurate unless we go to $N \to \infty$.

[1] M. A. Cazalilla, R. Citro, T. Giamarchi, E. Orignac, and M. Rigol, Rev Mod. Phys. **83**, 1405 (2011).

[2] B. Paredes, A. Widera, V. Murg, O. Mandel, S. Föling, I. Cirac, G. V. Shlyapnikov, T. W. Hänsch, and I. Bloch, Nature (London) **429**, 277 (2004).

[3] T. Kinoshita, T. Wenger, and D. S. Weiss, Science **305**, 1125 (2004).

[4] E. Haller, M. Gustavsson, M. J. Mark, J. G. Danzl, R. Hart, G. Pupillo, and H.-C. Nägerl, Science **325**, 1224 (2009).

[5] M. Olshanii, Phys. Rev. Lett. **81**, 938 (1998).

[6] M. D. Girardeau, E. M. Wright, and J. M. Triscari, Phys. Rev. A **63**, 033601 (2001).

[7] T. Papenbrock, Phys. Rev. A **67**, 041601(R) (2003).

[8] A. Minguzzi, P. Vignolo, and M. P. Tosi, Phys. Lett. A **294**, 222 (2002).

[9] M. Olshanii and V. Dunjko, Phys. Rev. Lett. **91**, 090401 (2003).

[10] W. Xu and M. Rigol, Phys. Rev. A **92**, 063623 (2015).

[11] F. Deuretzbacher, K. Fredenhagen, D. Becker, K. Bongs, K. Sengstock, and D. Pfannkuche, Phys. Rev. Lett. **100**, 160405 (2008).

[12] F. Deuretzbacher, D. Becker, J. Bjerlin, S. M. Reimann, and L. Santos, Phys. Rev. A **90**, 013611 (2014).

[13] A. G. Volosniev, D. V. Fedorov, A. S. Jensen, M. Valiente, and N. T. Zinner, Nat. Commun. **5**, 5300 (2014).

[14] L. Yang, L. Guan, and H. Pu, Phys. Rev. A **91**, 043634 (2015).

[15] L. Yang and X. Cui, Phys. Rev. A **93**, 013617 (2016).

[16] F. Deuretzbacher, D. Becker, and L. Santos, Phys. Rev. A **94**, 023606 (2016).

[17] T. Giamarchi, *Quantum Physics in One Dimension* (Oxford University Press, Oxford, 2004).

[18] F. D. M. Haldane, Phys. Rev. Lett. **47**, 1840 (1981); J. Phys. C: Solid State Phys. **14**, 2585 (1981).

[19] G. A. Fiete, Rev. Mod. Phys. **79**, 801 (2007).

[20] D. M. Stamper-Kurn and M. Ueda, Rev. Mod. Phys. **85**, 1191 (2013).

[21] G. Pagano, M. Mancini, G. Cappellini, P. Lombardi, F. Schäfer, H. Hu, X.-J. Liu, J. Catani, C. Sias, M. Inguscio, and L. Fallani, Nat. Phys. **10**, 198 (2014).

[22] J. Decamp, J. Jünemann, M. Albert, M. Rizzi, A. Minguzzi, and P. Vignolo, Phys. Rev. A **94**, 053614 (2016).

[23] V. V. Cheianov, H. Smith, and M. B. Zvonarev, Phys. Rev. A **71**, 033610 (2005).

[24] A. E. Feiguin and G. A. Fiete, Phys. Rev. B **81**, 075108 (2010).

[25] K. R. A. Hazzard, A. M. Rey, and R. T. Scalettar, Phys. Rev. B **87**, 035110 (2013).

[26] Z. Zhou, Z. Cai, C. Wu, and Y. Wang, Phys. Rev. B **90**, 235139 (2014).

[27] H. H. Jen and S.-K. Yip, Phys. Rev. A **94**, 033601 (2016).

[28] L. Tonks, Phys. Rev. **50**, 955 (1936).

[29] M. D. Girardeau, J. Math. Phys. **1**, 516 (1960).

[30] I. Shvarchuck, Ch. Buggle, D. S. Petrov, K. Dieckmann, M. Zielonkowski, M. Kemmann, T. G. Tiecke, W. von Klitzing, G. V. Shlyapnikov, and J. T. M. Walraven, Phys. Rev. Lett. **89**, 270404 (2002).

[31] M. J. Davis, P. B. Blakie, A. H. van Amerongen, N. J. van Druten, and K. V. Kheruntsyan, Phys. Rev. A **85**, 031604(R) (2012).

[32] T. Jacqmin, B. Fang, T. Berrada, T. Roscilde, and I. Bouchoule, Phys. Rev. A **86**, 043626 (2012).

[33] B. Fang, A. Johnson, T. Roscilde, and I. Bouchoule, Phys. Rev. Lett. **116**, 050402 (2016).

[34] M. Kozuma, L. Deng, E. W. Hagley, J. Wen, R. Lutwak, K. Helmerson, S. L. Rolston, and W. D. Phillips, Phys. Rev. Lett. **82**, 871 (1999).

[35] J. Stenger, S. Inouye, A. P. Chikkatur, D. M. Stamper-Kurn, D. E. Pritchard, and W. Ketterle, Phys. Rev. Lett. **82**, 4569 (1999).

[36] J. Steinhauer, R. Ozeri, N. Katz, and N. Davidson, Phys. Rev. Lett. **88**, 120407 (2002).

[37] S. B. Papp, J. M. Pino, R. J. Wild, S. Ronen, C. E. Wieman, D. S. Jin, and E. A. Cornell, Phys. Rev. Lett. **101**, 135301 (2008).

[38] G. Veeravalli, E. Kuhnle, P. Dyke, and C. J. Vale, Phys. Rev. Lett. **101**, 250403 (2008).

[39] J. M. Pino, R. J. Wild, P. Makotyn, D. S. Jin, and E. A. Cornell, Phys. Rev. A **83**, 033615 (2011).

[40] T. L. Ho, Phys. Rev. Lett. **81**, 742 (1998).

[41] T. Ohmi and K. Machida, J. Phys. Soc. Jpn. **67**, 1822 (1998).

[42] A. Lenard, J. Math. Phys. **5**, 930 (1964).

[43] H. G. Vaidya and C. A. Tracy, Phys. Rev. Lett. **42**, 3 (1979).

[44] M. Jimbo, T. Miwa, Y. Môri, and M. Sato, Physica D **1**, 80 (1980).

[45] P. J. Forrester, N. E. Frankel, T. M. Garoni, and N. S. Witte, Phys. Rev. A **67**, 043607 (2003).

[46] F. Dalfovo, S. Giorgini, L. P. Pitaevskii, and S. Stringari, Rev. Mod. Phys. **71**, 463 (1999).

[47] V. V. Cheianov and M. B. Zvonarev, Phys. Rev. Lett. **92**, 176401 (2004).

[48] G. A. Fiete and L. Balents, Phys. Rev. Lett. **93**, 226401 (2004).

[49] K. Penc, K. Hallberg, F. Mila, and H. Shiba, Phys. Rev. Lett. **77**, 1390 (1996).

[50] K. Penc and M. Serhan, Phys. Rev. B **56**, 6555 (1997).

[51] S. Tan, Ann. Phys. (NY) **323**, 2952 (2008).

[52] M. Barth and W. Zwerger, Ann. Phys. (NY) **326**, 2544 (2011).

[53] E. Braaten and L. Platter, Phys. Rev. Lett. **100**, 205301 (2008).

[54] E. Braaten, D. Kang, and L. Platter, Phys. Rev. A **78**, 053606 (2008).

[55] F. Werner, L. Tarruell, and Y. Castin, Eur. Phys. J. B **68**, 401 (2009).

[56] S. Zhang and A. J. Leggett, Phys. Rev. A **79**, 023601 (2009).

[57] F. Werner and Y. Castin, Phys. Rev. A **74**, 053604 (2006).

[58] F. Werner, Phys. Rev. A **78**, 025601 (2008).

[59] C. M. Bender and S. A. Orszag, *Advanced Mathematical Methods for Scientists and Engineers I: Asymptotic Methods and Perturbation Theory* (Springer-Verlag, New York, 1999).